Environmetrics

WILEY

RESEARCH ARTICLE OPEN ACCESS

Modeling Disease Dynamics From Spatially Explicit Capture-Recapture Data

Fabian R. Ketwaroo[1,2] | Eleni Matechou[2] | Matthew Silk[3,4,5] | Richard Delahay[6]

[1]Swiss Ornithological Institiue, Sempach, Switzerland | [2]School of Mathematics, Statistics and Actuarial Science, University of Kent, Canterbury, UK | [3]Institute of Ecology and Evolution, University of Edinburgh, Edinburgh, UK | [4]CEFE, University of Montpellier, CNRS, EPHE, IRD, Montpellier, France | [5]Centre for Ecology and Conservation, University of Exeter, Penryn, UK | [6]National Wildlife Management Centre, Animal & Plant Health Agency, Sand Hutton, York, UK

Correspondence: Fabian R. Ketwaroo (fabian.ketwaroo@vogelwarte.ch; f.ketwaroo@kent.ac.uk)

Received: 21 August 2023 | **Revised:** 9 October 2024 | **Accepted:** 6 November 2024

Keywords: density-dependent transmission | endemic disease | European badger | population density

ABSTRACT

One of the main aims of wildlife disease ecology is to identify how disease dynamics vary in space and time and as a function of population density. However, monitoring spatiotemporal and density-dependent disease dynamics in the wild is challenging because the observation process is error-prone, which means that individuals, their disease status, and their spatial locations are unobservable, or only imperfectly observed. In this paper, we develop a novel spatially-explicit capture-recapture (SCR) model motivated by an SCR data set on European badgers (*Meles meles*), naturally infected with bovine tuberculosis (*Mycobacterium bovis*, TB). Our model accounts for the observation process of individuals as a function of their latent activity centers, and for their imperfectly observed disease status and its effect on demographic rates and behavior. This framework has the advantage of simultaneously modeling population demographics and disease dynamics within a spatial context. It can therefore generate estimates of critical parameters such as population size; local and global density by disease status and hence spatially-explicit disease prevalence; disease transmission probabilities as functions of local or global population density; and demographic rates as functions of disease status. Our findings suggest that infected badgers have lower survival probability but larger home range areas than uninfected badgers, and that the data do not provide strong evidence that density has a non-zero effect on disease transmission. We also present a simulation study, considering different scenarios of disease transmission within the population, and our findings highlight the importance of accounting for spatial variation in disease transmission and individual disease status when these affect demographic rates. Collectively these results show our new model enables a better understanding of how wildlife disease dynamics are linked to population demographics within a spatiotemporal context.

1 | Introduction

Understanding relationships between the dynamics of populations and their infectious pathogens is a key aim of wildlife disease ecology. Infectious diseases can directly influence population density through impacts on demographic vital rates (Manlove et al. 2016; McCallum et al. 2007; Vredenburg et al. 2010), but in turn disease dynamics can vary in space and time as well as with population density. Quantifying how pathogen transmission varies with population density is important because of its implications for the conservation and management of wildlife populations (McCallum 2016; Silk et al. 2019). Hereafter, we refer to pathogen transmission as disease transmission. While the potential importance of host

density for epidemiological dynamics has long been known (Krkošek 2010; O'Neill et al. 2023), it is now recognized that aspects of spatial and social behavior (e.g., Albery et al. 2021) can mean that disease transmission may covary with host population density across a continuum from density-dependent (transmission increases with population density) to frequency-dependent (transmission is independent of population density) (Hopkins et al. 2020).

There are two main analytical challenges associated with quantifying the relationship between host density and disease transmission in wildlife populations. First is the difficulty of estimating population size, and hence population density, in wild populations, where not every individual is captured or observed over time. The second challenge is associated with the detection of infection in wild hosts owing to limitations in the sensitivity and specificity of diagnostic tests (Choquet et al. 2013; Drewe et al. 2010; Enøe, Georgiadis, and Johnson 2000).

Capture-recapture (CR) models have been one of the main tools developed to estimate the population size of wild animals. Traditional CR models essentially represent "fish bowl" sampling, that is, a system that is unconnected to the spatial structure of the population. These models do not account for the spatial nature of sampling nor the spatial distribution of individuals (Royle, Fuller, and Sutherland 2018). Consequently, they do not allow for the study of many vital spatial population processes, such as density, movement, and dispersal of individuals. This weakness of CR models has been overcome by the development of spatially-explicit capture-recapture (SCR) models (Borchers and Efford 2008; Efford 2004). SCR models consider the collection of individuals in a population as a latent point process, with each point corresponding to an individual activity center (AC), defined as the core of its home range area. Home range area refers to the area an individual typically occupies and traverses in its activities such as foraging, mating, or nesting.

In SCR data, individual ACs are unknown and thus are considered latent variables in corresponding models. SCR models can be fitted in a classical framework, where the ACs are marginalized from the likelihood by integration (Borchers and Efford 2008), or in a Bayesian framework, where the ACs are explicitly estimated along with other unknown parameters and random variables using Markov chain Monte Carlo (MCMC) methods (J. A. Royle and Young 2008). Once inferred, the ACs can be used to estimate spatial population processes such as density, which is the number of ACs per unit area of the region of interest. Additionally, conditional on the latent ACs, the probability of observing or encountering an individual is modeled as a function of the distance between the individual's AC and the location of each trap. Consequently, SCR models take into consideration the spatial nature of sampling as well as the spatial distribution of individual ACs to allow for the study of spatial population processes. This is arguably equally important to the study of demographic population rates, with the formal link between state model and observational model allowing for better inference on the former and more robust accommodation of the latter (Sutherland, Royle, and Linden 2019). When data are collected over a longer time frame, for example over multiple years or seasons, open SCR models (Gardner et al. 2010) can be used to estimate demographic population rates such as survival and recruitment in addition to spatial population processes.

However, existing SCR models do not currently accommodate additional data on the disease status of captured individuals. These data typically consist of diagnostic test results that are also prone to error and hence are only an imperfect observation of an individual's disease status. In addition, as is always the case in CR data, these individual-level diagnostics are only available for the particular time point when an animal is captured, and are missing for all other times and for individuals that have never been caught.

In the present study, we develop a novel open SCR model that accounts for the observation process of individuals, as well as their imperfectly observed disease status. Our new modeling framework allows the simultaneous modeling of population demographics and disease dynamics within a spatiotemporal context. This makes it possible to simultaneously test hypotheses related to spatial and density-related variation in disease transmission while examining variation in survival and individual capture probabilities as a function of individual (latent) disease state.

We perform a simulation study to assess model performance for a number of scenarios. Our results reveal the requirement in terms of effect size to have sufficient power to identify density-dependence in disease transmission. Finally, our study indicate that when demographic rates are dependent upon individual disease status, existing SCR models, which do not account for that dependence, yield substantially biased estimates of population density.

We then fit our model to a motivating case study of European badgers (*Meles meles*), naturally infected with bovine tuberculosis (*Mycobacterium bovis*, TB) at Woodchester Park in Gloucestershire, UK (Delahay et al. 2013; McDonald, Robertson, and Silk 2018), revealing important aspects of the epidemiological dynamics. Our model reveals that infected individuals have a lower survival probability and larger home range areas. We also infer that, despite a more recent reduction in population size, the prevalence of infection remained constant and that the data do not provide strong evidence that density has a non-zero effect on disease transmission. The paper is structured as follows: in Section 2 we describe the case study that motivated the work in this paper, in Section 3 we introduce the new model and discuss our inference approach, while Sections 4 and 5 present simulation and case study results, respectively. Section 6 discusses the results from our simulations and case study in the context of wildlife disease ecology, and suggests directions for future work.

2 | Data Collection and Processing

The Woodchester Park study area is located on the Cotswold limestone escarpment in Gloucestershire, South West England. Over an area of ~7 km^2 the resident badger population has been monitored in a consistent manner since 1981 (McDonald, Robertson, and Silk 2018). The majority of the study area comprises mixed woodland, grassland, and arable farmland (Delahay et al. 2006). Badger population density is relatively high (Rogers et al. 1997) and their social groups occupy more or less contiguous territories

throughout the study area (Delahay et al. 2006), each of which is typically associated with one main sett and several smaller outlying setts (underground burrow systems).

The badger population is monitored by CR sampling, which enables the collection of demographic and epidemiological data. The study area has been divided into three zones of approximately equal size, each of which is trapped four times per year from May to January inclusive, with a suspension from February to April to avoid catching dependent cubs and their mothers (Woodroffe et al. 2006). To determine which setts are active and how many traps to deploy, a sett activity survey is conducted in each zone before each trapping event. At each active sett, more traps are deployed than are expected to be required (i.e., avoiding saturation trapping).

Box traps constructed of steel mesh are dug into the substrate close to each active sett and baited with peanuts for 4 to 8 days to habituate badgers to their presence (Cheeseman and Harris 1982). On the last day of baiting, the traps are set for two consecutive nights and are checked on the following mornings. Once captured, newly caught badgers are aged, sexed and permanently marked with a unique ID tattoo on the abdomen (Cheeseman and Harris 1982), with their weight, body condition, body length, reproductive status, and tooth wear recorded at this and every subsequent capture event.

Once captured, three tests are used to determine their TB status: interferon-gamma immunoassay (Ifn, Dalley et al. 2008), used since 2006 to detect a cell-mediated immune response, Dual Path Platform test (DPP®, Chembio.inc), used since 2014 to test for antibodies (Ashford et al. 2020) and selective microbiological culture of clinical samples (Cul, Gallagher and Horwill 1977) used since 1976. Ifn and DPP® use blood samples while Cul is carried out on samples of sputum, feces, urine, and swabs of abscesses and wounds. Each test is imperfect, resulting in false positive and false negative errors, making it difficult to infer an individual's disease state from the tests alone (Drewe et al. 2010).

Following examination and collection of diagnostic samples, badgers caught during the first night of trapping are held overnight and released the following morning to prevent them from being re-captured on the second trapping night. Badgers caught during the second night are released the following day. Badgers are released where captured, following a period of recovery and subject to a welfare assessment.

3 | Model

Open SCR models follow the robust design (Pollock 1982) and assume that a population of $i = 1, \ldots, N_t$ individuals is monitored at $t = 1, \ldots, T$ primary periods, each having $r = 1, \ldots, R$ secondary sampling occasions at $j = 1, \ldots, J$ sampling locations. The population is open to births/death/immigration/emigration between primary periods but closed across the R sampling occasions within each period. Each individual has an associated spatial location within a spatial domain (S), representing its AC $s_{i,t}$, a two-dimensional spatial coordinate. The collection of ACs can be thought of as a statistical spatial point pattern that describes how individuals are distributed within S. This statistical point process is often referred to as the state model. Here, we define our model in a Bayesian framework using data augmentation (Royle and Dorazio 2012) and let $i = 1, \ldots, M$ be "pseudo-individuals" that potentially could belong to N_t.

Our model has two key latent states: presence, $z_{i,t}$, and disease status, $d_{i,t}$, defined as

$$z_{i,t} = \begin{cases} 1 & \text{alive in primary period t} \\ 0 & \text{unrecruited/dead in primary period t} \end{cases}$$

$$d_{i,t} \mid z_{i,t} = 1 = \begin{cases} 1 & \text{infected given alive in primary period t} \\ 0 & \text{uninfected given alive in primary period t} \end{cases}$$

We assume that individual ACs do not change over time by modeling

$$s_{i,t} = s_i \sim \text{Uniform}(S) \;\; \forall i, t$$

Following the data collection and processing methods described in Section 2, we assume that an individual can be caught in maximum one sampling location on a secondary sampling occasion, but that each sampling location can catch more than one individual at a time (Efford, Borchers, and Byrom 2009; Ergon and Gardner 2014). Let $y_{i,r,t}$ denote the index of the sampling location where individual i is captured in secondary occasion r within a primary occasion t, and $y_{i,r,t} = 0$ when an individual is not captured. The observation likelihood is

$$y_{i,r,t} \sim \text{Categorical}\left(\pi_{i,r,t}\right)$$

where $\pi_{i,r,t}$, the sampling location and individual specific capture probability, is a $1 \times (J+1)$ vector with the first element being the probability of not being captured and the remaining elements being the probability of capture in 1 to J sampling locations. Following Ergon and Gardner (2014), we allow sampling location-specific capture probabilities to depend on the locations of all other sampling locations and to decline with the distance between the AC of the individual and the sampling location. Let $h_{i,r,t,j}$ denote the capture hazard rate of individual i during sampling occasion (r, t) in sampling location j and $h_{i,r,t,*} = \sum_j h_{i,r,t,j}$ be the total risk of being captured in any sampling location. The probability of not being captured in any sampling location is

$$\pi_{i,r,t}[1] = \exp\left(-h_{i,r,t,*} z_{i,t}\right)$$

and the probability of being captured in sampling location j is

$$\pi_{i,r,t}[j+1] = \left(1 - \pi_{i,r,t}[1]\right) \frac{h_{i,r,t,j}}{h_{i,r,t,*}}$$

To model $h_{i,r,t,j}$, we use the hazard half-normal function (Royle et al. 2013).

$$h_{i,r,t,j} = \lambda_{d_{i,t}} \exp\left(-\frac{1}{2\sigma^2_{d_{i,t}}} \left\| x_{r,t,j} - s_i \right\|^2 \right)$$

where $x_{r,t,j}$ is the two-dimensional spatial coordinate location of the j th sampling location during sampling occasion (r, t), $\lambda_{d_{i,t}} > 0$ is the baseline encounter rate and $\sigma_{d_{i,t}} > 0$ represents the rate at which capture probability declines as the Euclidean distance

from the AC increases. We model both of these parameters dependent on the individual disease status in primary period t, using log-linear models for λ and σ, both of which have the binary disease status as the only covariate, allowing disease status to potentially affect behavior in terms of space use.

Finally, we model the result of test Q, $\omega_{i,t}^{Q}$, for individual i on occasion t, conditional on their disease status, as a Bernoulli $\left(\omega_{i,t}^{Q}\right)$ random variable, with

$$\omega_{i,t}^{Q} \mid d_{i,t} = \begin{cases} 1 - q_{00}^{Q}, & d_{i,t} = 0 \\ q_{11}^{Q}, & d_{i,t} = 1 \end{cases}$$

where we refer to the probability of a true positive result by test Q as q_{11}^{Q} (sensitivity of test Q) and to the corresponding probability of a true negative result as q_{00}^{Q} (specificity of test Q), and $Q \in \{\text{DPP}^{®}, \text{Ifn}, \text{Cul}\}$. Following Buzdugan et al. (2017), we assume independence between tests and hence define the joint distribution of the three test results as the product of the marginal Bernoulli distributions. The sensitivity and specificity of each test are inferred parameters, thus, enabling the diagnostic accuracy of each test to be evaluated. This formulation accounts for imperfect tests and enables a higher diagnostic accuracy than single-test use (Drewe et al. 2010).

We model the transition between latent states accordingly, so that at $t = 1$

$$z_{i,1} \sim \text{Bernoulli}\left(\gamma_1\right)$$
$$d_{i,1} \mid z_{i,1} \sim \text{Bernoulli}\left(z_{i,1}\delta_I\right)$$

where γ_1 is the recruitment probability that a "pseudo-individual" is in the population at the start of the study and δ_I is the probability of being infected at the start of the study. For $t \geq 2$,

$$z_{i,t} \sim \text{Bernoulli}\left(\phi_{d_{i,t-1}} z_{i,t-1} + \gamma_t \alpha_{i,t}\right)$$
$$d_{i,t} \sim \text{Bernoulli}\left(z_{i,t}\left[d_{i,t-1} + \left\{\left(1 - d_{i,t-1}\right)\psi_{i,t-1}\right\}\right]\right)$$

where $\phi_{d_{i,t-1}}$ is the probability of survival from primary period $t-1$ to t conditional on disease status in primary period $t-1$ for individual i, $\psi_{i,t}$ is the disease transmission probability, that is the probability that an individual that is uninfected in primary period $t-1$ becomes infected by primary period t, γ_t is the recruitment probability that a "pseudo-individual" is first recruited, and hence is first available for capture, in primary period t and $\alpha_{i,t}$ is a latent indicator variable of whether an individual is available to be recruited or not in primary period t. We define $\alpha_{i,t} = \left(1 - \text{I}\left(\sum_{t=1}^{t-1}\left(z_{i,t}\right) > 0\right)\right)$ such that $\alpha_{i,t} = 1$ if individual i is available to be recruited in primary period t, $\alpha_{i,t} = 0$ otherwise to ensure an individual can only be recruited once.

We note that, clearly, only individuals that are alive and uninfected can become infected and, as is the case in our motivating data, once infected, individuals cannot become uninfected. To investigate the relationship between density and disease transmission, we model $\psi_{i,t}$ as a function of local population density at each primary period. We discretize the study space using a grid and create G non-overlapping habitat cells. We denote the cell in which individual AC i falls by c_i, with $c_i \in \{1, \ldots, G\}$. Local density of grid cell g, $g = 1, \ldots, G$, on occasion t is defined as $\ell_{g,t} = \sum_{i=1}^{M} I\left(z_{i,t} = 1, c_i = g\right)$, where $I\left(z_{i,t} = 1, c_i = g\right)$ is an indicator variable equal to 1 if individual i is alive in primary period t and its AC falls within cell g, and 0 otherwise. Therefore, $\ell_{g,t}$ corresponds to the number of live individuals with ACs in cell g in primary period t. Thus, we build a logistic regression model for the probability of disease transmission

$$\text{logit}\left(\psi_{i,t}\right) = \beta_0 + \beta_1 \ell_{c_i,t} \tag{1}$$

such that an uninfected individual can become infected due to the local density $\left(\ell_{c_i,t}\right)$ at the individual AC location in its habitat cell. Coefficient β_1 determines the direction and size of the effect of local density on disease transition probability.

Finally, population size in primary period t, N_t, is defined as $N_t = \sum_i z_{i,t}$ and corresponding global population density, D_t, as $D_t = N_t/\text{area}(S)$, while the corresponding sizes of the infected population (N_t^{i}) and of the uninfected population $\left(N_t^{\text{u}}\right)$ as $N_t^{\text{i}} = \sum_i z_{i,t} d_{i,t}$ and $N_t^{\text{u}} = \sum_i z_{i,t}\left(1 - d_{i,t}\right)$, respectively. Hence, disease prevalence (D_t^{i}) is defined as $D_t^{\text{i}} = N_t^{\text{i}}/N_t$. Density, global and local, is latent, and throughout the manuscript, we refer to it as density.

We fit models in a Bayesian framework using MCMC methods via R package NIMBLE (de Valpine et al. 2017) version 1.2.1. Additionally, to increase the computational efficiency of using a Bayesian implementation via data augmentation, we vectorize computation and perform block sampling on correlated parameters (Turek et al. 2021) when appropriate. We employ user-defined NIMBLE functions to reduce the total number of nodes in the model and improve MCMC efficiency. We use the R package nimbleSCR (Bischof et al. 2020) version 0.2.1 to create habitat grids and for the computation of local density. To improve convergence and mixing, we use a fine habitat grid to provide the model with a large number of latent density points to serve as a covariate on disease transmission probability. We also center latent density to improve computation by reducing the correlation between the intercept and fixed effect. Random walk block samplers are assigned to $(q_{11}^{\text{DPP}^{®}}, q_{11}^{\text{Ifn}}, q_{11}^{\text{Cul}})$, $(q_{00}^{\text{DPP}^{®}}, q_{00}^{\text{Ifn}}, q_{00}^{\text{Cul}})$ and $\left(\lambda_{d_i}, \sigma_{d_i}\right)$ to improve MCMC efficiency. The code is freely available on https://github.com/Fabian-Ketwaroo/Modelling-disease-dynamics-from-spatially-explicit-capture-recapture-data. The data from the Woodchester Park study can be made available on request to the Animal and Plant Health Agency via Richard Delahay.

4 | Simulation Study

We performed a simulation study to assess the performance of the proposed modeling framework in estimating population density and all other model parameters, as well as the impact on estimation when the effect of (local) population density on transmission probability is ignored and, more importantly, when density-dependent disease transmission, disease status and its effect on other model parameters are ignored altogether. We refer to our proposed model as $\text{M}\left(\psi_\ell\right)$, to the model that does not account for density-dependence in ψ as model $\text{M}\left(\psi_0\right)$ and to the standard open SCR model that does not account for density dependence and disease status as model M(SRC0).

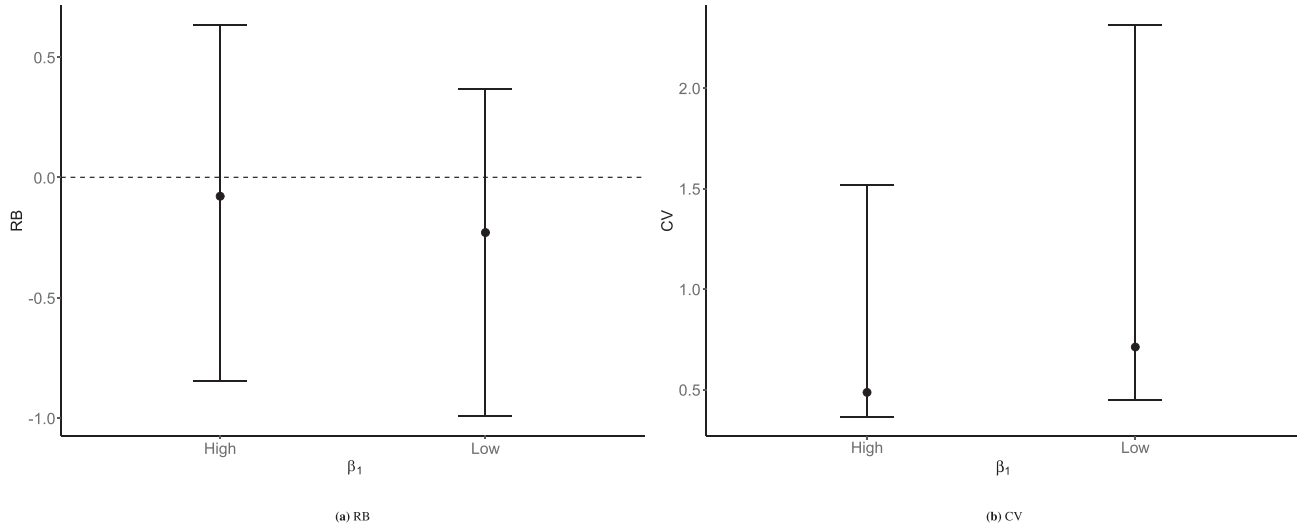

FIGURE 1 | 95% quantile error bars of RB, (a), and CV, (b), for β_1 when using our proposed model, $\mathrm{M}(\psi_{\ell})$. Dots represent the median in each case.

We investigate model performance at both high and low density effects on disease transmission, $\beta_1 = (0.5,0.25)$. We motivated our simulation study using parameter values similar to those obtained from the case study analysis. We set $M = 500, T = 8, R = 3$ and the rest of the parameter values as: $\phi_{d_i=0} = 0.9$, $\phi_{d_i=1} = 0.8$, $\gamma_1 = 0.4$, $\gamma_{2:4} = 0.1$, $\gamma_5 = 0.2$, $\gamma_{6:T} = 0.15$, $\lambda_{d_i=0} = 1.5$, $\lambda_{d_i=1} = 0.25$, $\sigma_{d_i=0} = 0.25$, $\sigma_{d_i=1} = 0.6$, $\delta_I = 0.15$, $\beta_0 = -3$, $q_{11}^{\mathrm{DPP}^{\circledast}} = 0.492$, $q_{11}^{\mathrm{Ifn}} = 0.809$, $q_{11}^{\mathrm{Cul}} = 0.1$, $q_{00}^{\mathrm{DPP}^{\circledast}} = 0.931$, $q_{00}^{\mathrm{Ifn}} = 0.936$, and $q_{00}^{\mathrm{Cul}} = 0.999$. This setting results in mean local density ≈ 4.2, which is very close to that of the case study.

We used a 9×5 habitat grid in which we centered the case study sampling locations. For each case, we performed 30 simulation runs and used relative bias $\left(\mathrm{RB} = \frac{\bar{\theta}-\theta}{\theta}\right)$ to measure relative error and coefficient of variation $\left(\mathrm{CV} = \frac{\mathrm{SD}(\hat{\theta})}{|\bar{\theta}|}\right)$ to measure relative precision, where θ is the true parameter value, $\bar{\theta}$ is the mean and $\mathrm{SD}(\hat{\theta})$ is the standard deviation of the posterior distribution obtained, across the 30 runs. Further details on the simulation study are given in Section S1.

From Figure 1 and Table S2, we can see that as expected, the quality of inference of the density effect (β_1) is highest when the density effect is high, with RB and CV smaller than when the density effect is low (Figure 1). This highlights that reliable inference of β_1 is possible but is more challenging than for other parameters, as also reported by Milleret et al. (2023). In addition, as shown in Figure 2, N_t is inferred similarly well at both density levels, N_t^{i} is inferred with lower CV in the high-density level case and N_t^{u} with lower CV in the low-density level case.

From Figure 2, it can be seen that, for the early primary periods in particular, the M(SCR 0) model has a negative RB for N, whereas the opposite is true for the $\mathrm{M}(\psi_0)$ at both levels of density effect. The simpler M(SCR 0) model has a lower CV compared to the two more complicated models, especially at the high-density level. All three models have similar CV for N with higher CV values at the start and end of the study period. This result highlights the need to account for the spatial variation in disease transmission and the disease status of individuals where these are linked to demographic parameters and/or space use. As shown in Figure S1, we simulated the density values, which serve as the latent covariate in model $\mathrm{M}(\psi_{\ell})$, using a realistic scenario of small and gradual changes, with ACs simulated from a homogeneous Poisson process, as is the standard assumption of SCR models, including the one in this paper. As a result, especially when the true value for β_1 is low, density does not vary dramatically between primary periods or between grid cells, and hence, ignoring its effect in the $\mathrm{M}(\psi_0)$ model does not lead to substantial bias in the estimation of N.

5 | Case Study

We analyzed SCR data and corresponding disease test data collected from 2014 to 2018 by the long-term study at Woodchester Park using the modeling framework defined in Section 3. These years were selected as they correspond to a period when the population was undisturbed by management interventions and the diagnostic tests for TB did not change, as opposed to the previous years where different tests were employed and subsequent years when badger culling for TB control was initiated in the surrounding area. Closure was assumed within each of the four times the three zones were sampled across the years, but open between the four primary periods across the years. We use $M = 1500$ and an 11×8 habitat grid in which we center the sampling locations. Prior settings are provided in Section S2.3 where informative priors for the sensitivity and specificity of each test were elicited from Drewe et al. (2010) and Ashford et al. (2020).

Table 1 displays key posterior estimates obtained. Caterpillar plots of these parameter posterior distributions are also shown in Section S2.4. All parameters converged according to Gelman and Rubin's convergence diagnostic (Gelman and Rubin 1992), displayed good mixing, and had effective sample size (ESS) ≥ 200 except the intercept of disease transmission which has ESS ≈ 110.

Figure 3a indicates that during the study period (2014–2018) the Woodchester badger population was in decline, with both

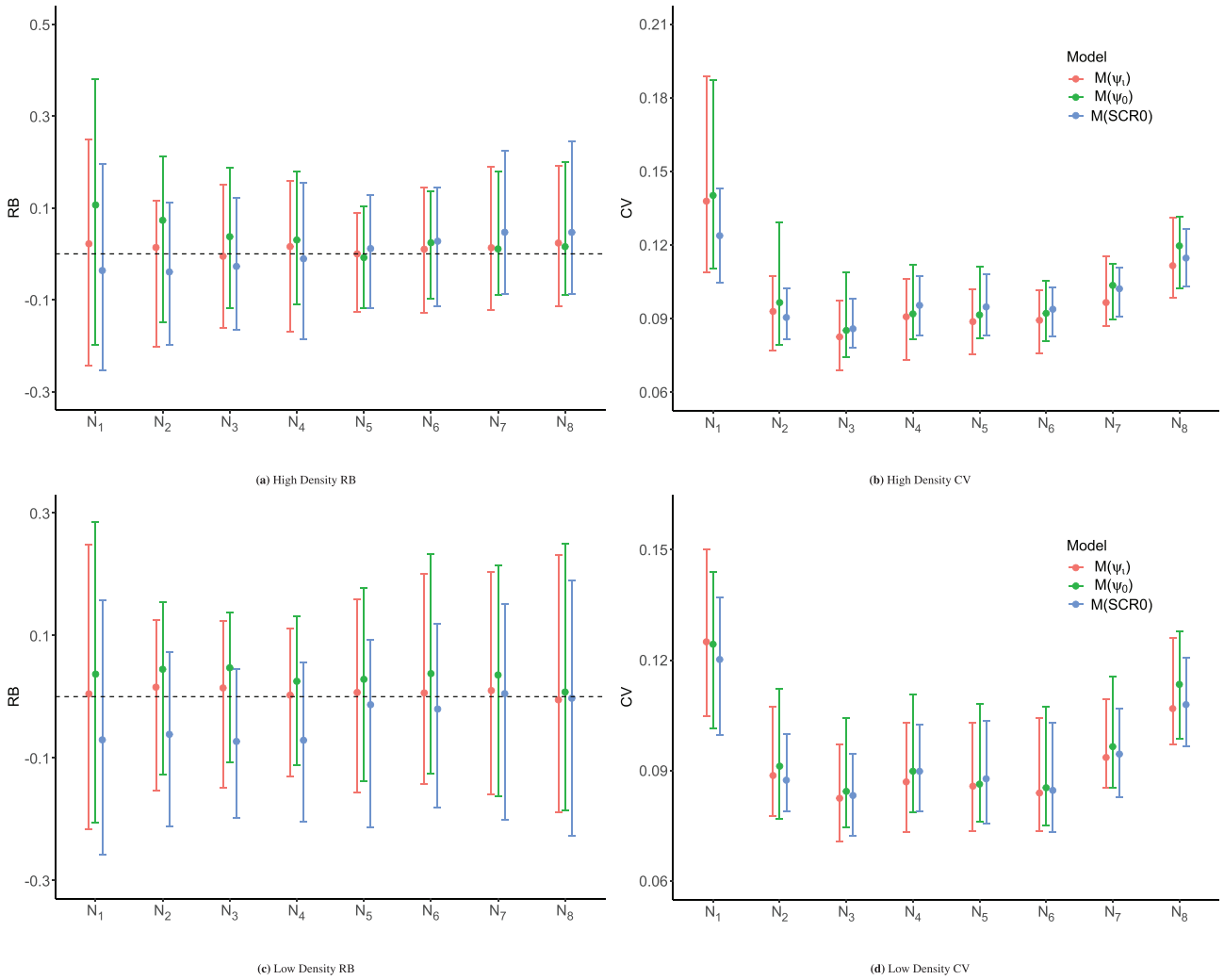

FIGURE 2 | 95% quantile error bars of RB and CV of population size, N, at high and low-density effect levels for three models: Our proposed model, $\mathrm{M}(\psi_\ell)$, the model that does not account for density-dependence in disease transmission, $\mathrm{M}(\psi_0)$ and the model that does not account for disease status, M(SCR 0). Dots represent the median in each case.

the number of uninfected and infected individuals decreasing over the course of the study. Disease prevalence during this period remained relatively stable with median disease prevalence between 20% and 25% (Figure 3b). Additionally, our model output includes posterior distributions of the number of individuals newly infected on each sampling occasion (Figure S14), which in this case is shown to be decreasing, in line with the decreasing population size.

Model results also confirmed known differences between uninfected and infected badgers in relation to their behavior and survival, indicating that the latter were less likely to be captured at their activity center and had a larger home range area than the former, with 95% PCI of the difference between baseline encounter rates and of the scale parameter (1.082,1.745) and (−0.397, −0.2490), respectively.

Infected individuals also had a lower survival probability (ϕ) than uninfected individuals (Table 1), with the 95% PCI of the difference (0.038,0.182) excluding zero. Overall, the survival probability of infected individuals was approximately 10% lower than for uninfected individuals, albeit with more error around this estimate—potentially caused by the smaller sample size of infected individuals or greater variability in their survival. The sensitivity (q_{11}) and specificity (q_{00}) estimates for each test also provide valuable information on test performance. Specifically, Cul was found to have low sensitivity (23.4%) but had the highest specificity (99.1%), Ifn was the most sensitive (65.6%) and had relatively high specificity (90.7%), whereas the DPP® had intermediate sensitivity (52.0%) and very high specificity (97.8%). These estimates are similar to those obtained by Ashford et al. (2020) for DPP® and Drewe et al. (2010) for Ifn and Cul, and reflect known differences in the performance of the tests and the biological processes being targeted (e.g., Ifn detecting an initial cellular response to infection while Cul detects bacterial shedding by infectious individuals). Hence, the tests may, in some cases, be identifying animals at different stages of infection.

As individual latent ACs are estimated by the model, they enable useful and interesting summaries such as "realized kernel density maps" shown in Figure 4. These maps provide useful visualization of the distribution of individual ACs across the trapping grid,

TABLE 1 | Case study: Posterior distribution summaries of model parameters.

Parameters	Median	SD	95% PCI
γ_1	0.365	0.034	(0.300,0.435)
$\gamma_{2:4}$	0.020	0.011	(0.002,0.045)
γ_5	0.167	0.037	(0.099,0.248)
$\gamma_{6:8}$	0.010	0.008	(0.004,0.030)
γ_9	0.087	0.035	(0.030,0.165)
$\gamma_{10:12}$	0.048	0.018	(0.017,0.089)
γ_{13}	0.188	0.053	(0.099,0.305)
$\gamma_{14:16}$	0.017	0.015	(0.006,0.056)
$\phi_{d_i=0}$	0.892	0.012	(0.867,0.915)
$\phi_{d_i=1}$	0.792	0.033	(0.725,0.855)
$\lambda_{d_i=0}$	1.584	0.161	(1.302,1.929)
$\lambda_{d_i=1}$	0.220	0.044	(0.149,0.317)
$\sigma_{d_i=0}$	0.266	0.008	(0.251,0.283)
$\sigma_{d_i=1}$	0.588	0.038	(0.522,0.667)
δ	0.232	0.052	(0.140,0.342)
β_0	−2.878	0.350	(−3.698, −2.253)
β_1	−0.136	0.157	(−0.472,0.147)
$q_{11}^{\mathrm{DPP}^*}$	0.520	0.026	(0.471,0.573)
q_{11}^{Ifn}	0.656	0.038	(0.587,0.730)
q_{11}^{Cul}	0.234	0.035	(0.175,0.311)
$q_{00}^{\mathrm{DPP}^*}$	0.978	0.007	(0.961,0.990)
q_{00}^{Ifn}	0.907	0.013	(0.879,0.931)
q_{00}^{Cul}	0.991	0.005	(0.978,0.998)

making it easier to identify patterns, trends, and areas of high/low probability densities of individual ACs. Figure 4 displays the population kernel density maps for infected and uninfected individuals across years in spring after cubs have been recruited to the population. These plots are standardized across years with the black dots representing the setts trapped. The process used to obtain these maps is outlined in Section S2.5. These outputs reveal spatiotemporal variation in the distribution of uninfected and infected individuals across the population. High probability densities of infected badgers were concentrated in the central (and northern) and western area of the study site at the start of our study period, becoming more diffuse over time. The eastern parts of the study site maintained consistently higher probability densities of uninfected badgers throughout the period.

Finally, the data did not provide strong evidence that density has a non-zero effect on disease transmission. The simplistic interpretation would be that transmission was independent of local population density during our study period. However, density is a latent variable with an unknown effect, and hence the power to detect small effects relies heavily on the number of primary periods and the number of individuals becoming infected. Consequently, we can interpret this finding as evidence that strong density-dependence of transmission is highly unlikely, but that transmission could instead either be weakly density-dependent or close to frequency-dependent.

6 | Discussion

We have developed a novel SCR model that uses disease data from multiple imperfect tests together with SCR data to simultaneously model population demographics and disease dynamics within a spatiotemporal context. Accounting for observation error in both the individual capture process and the disease testing process, our modeling approach accounts for spatial variation in survival and individual capture probabilities as a function of individual (latent) disease state as well as variation in disease transmission as a function of population density. This allows for a better understanding of how disease dynamics relate to demography in a spatiotemporal context.

We also conducted a simulation study to assess model performance for a number of scenarios. Our simulations generated encouraging results for our modeling approach and highlighted that, if spatial variation in disease transmission and heterogeneity in demographic rates (capture and survival probabilities) induced by individual disease status are not accounted for, biased estimates of population size can be produced. Notably, there are existing models that use finite mixtures to model heterogeneity in these demographic rates (Pledger, Pollock, and Norris 2010). We have not considered these models but it is likely that they might return similar inference on population density to our proposed model. However, such models do not provide information on density-dependent disease transmission or information on individual disease status effects on such demographic parameters.

Applying this new model to a dataset on European badgers, naturally infected with TB, our model provided valuable insights into the badger-TB system with broader implications for wildlife disease ecology in general. Our model results agreed closely with previous findings from the Woodchester Park study system. Estimates of population size align with those from the long-term study (Delahay et al. 2013; McDonald, Robertson, and Silk 2018) and support the observed recent decline, while our estimates of individual badger home range area are similar to those from previous studies of this population (Garnett, Delahay, and Roper 2005; Tuyttens et al. 2000; Weber, Bearhop et al. 2013). Finally, our estimates of disease prevalence and incidence, as well as disease-associated changes in survival are similar to those found previously for this study population (prevalence: Delahay et al. 2013; incidence and changes in survival: Graham et al. 2013). However, the approach considered in this paper is the first to simultaneously model all these processes from the available SCR data and hence properly account for uncertainty in every stage of the process. Joint modeling of different data sets has been shown to improve parameter estimation, increase inference power, account for multiple sources of error, and so forth (Fletcher et al. 2016; Gotway and Young 2002; Schaub and Abadi 2011).

One key advantage of our modeling framework is that by using longitudinal diagnostic test results to infer the (unobservable) disease status of an individual, we are able to gain new insights into how individual movement patterns vary with disease status. Specifically, our results show that infected badgers ranged over larger areas than uninfected badgers. Previous research has detected a tendency for test-positive individuals (i.e., those likely

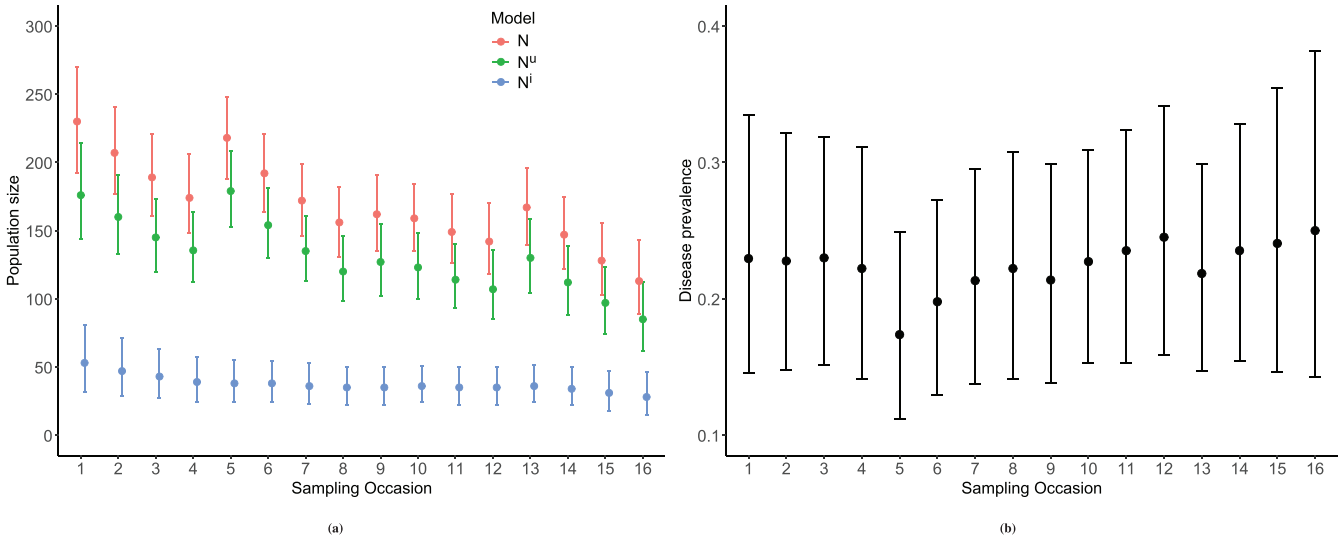

FIGURE 3 | 95% quantile error bars of, (a) total (N_t), uninfected (N_t^u), infected (N_t^i) population size, and (b) disease prevalence. Dots represent the posterior median.

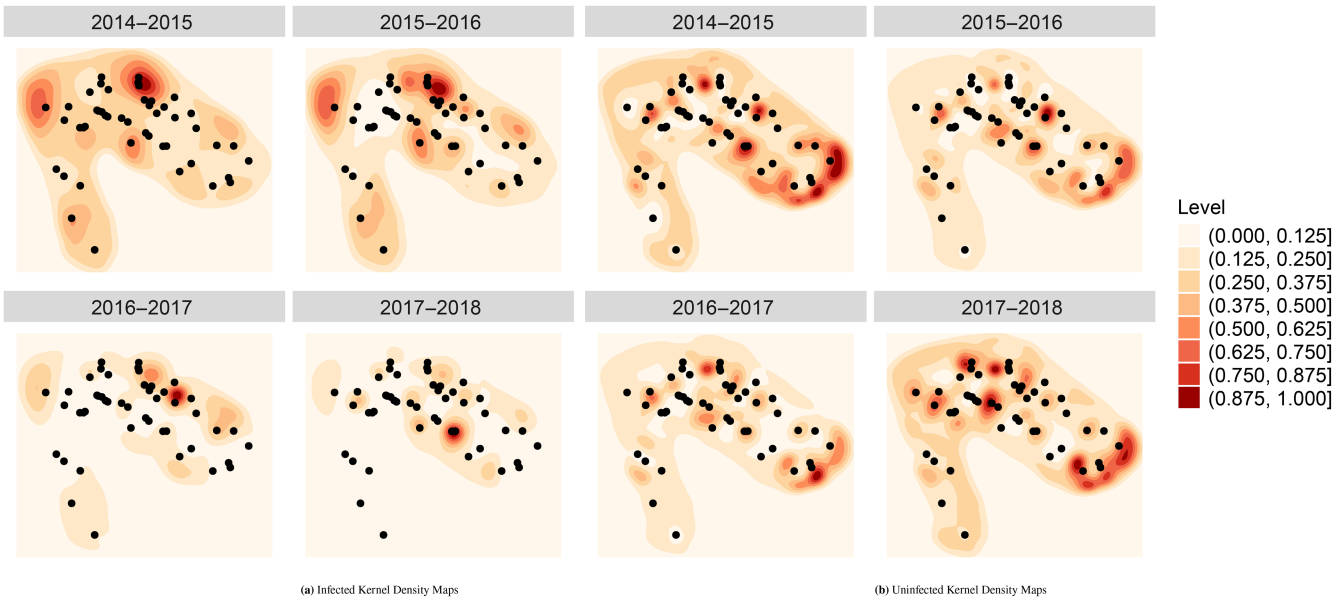

FIGURE 4 | Standardized kernel density maps for infected, (a) and uninfected, (b) individuals across years in Spring each year. Black dots represent the setts trapped and higher level values indicate higher probability density and vice-versa.

to be infected) to make greater use of outlying setts (Weber, Bearhop et al. 2013) and have more between-group contacts (Silk et al. 2018; Weber, Carter et al. 2013), both of which are traits expected to be linked to wider ranging behavior. Our model results indicate these changes may (to some extent) be linked directly to infection. The tendency for infected badgers to start ranging further likely has important implications for the epidemiology of the badger-TB host-pathogen system. Due to the modular nature of badger contact networks (Rozins et al. 2018), movements between groups offer important opportunities for transmission that enable wider pathogen spread. Therefore, changes in the behavior of infected badgers could play an important role in the longer-term persistence of the disease. Previous research in the Woodchester system has revealed a positive association between new individuals arriving in a group and the incidence of disease (Vicente et al. 2007). Infected badgers ranging over larger areas than uninfected badgers, using areas that are larger than typical social group territory size, would provide a mechanism to explain these findings.

Our results also add to our knowledge of how transmission scales with population density in the badger-TB system. We find no clear relationship between local population density and the incidence of infection in the Woodchester Park badger population (Delahay et al. 2005; Delahay et al. 2013). Historically, many infections that spread by (nonsexual) close contact were assumed to exhibit density-dependent (as opposed to frequency-dependent) transmission, and this principle of density-dependence underpins some interventions to control disease in wildlife populations (Carter et al. 2009; McCallum 2016). More recently, studies have

typically considered a continuum between frequency-dependent and density-dependent transmission driven by changes in individual behavior (Hopkins et al. 2020). For example, our failure to detect evidence for density-dependent transmission supports other research suggesting it may be that the transmission of many infectious diseases including TB is a function of population density at low population densities (i.e., density-dependent) but independent of it (i.e., frequency-dependent) at high population densities (Hu, Nigmatulina, and Eckhoff 2013). Our results fit well with this general pattern given that the Woodchester Park badger population was relatively high density during the study period, compared with badger populations elsewhere. At this population scale, it is likely that the social structure of the population plays an important role and it would be valuable for future research to focus on this question at finer social and spatial scales.

By separately estimating the density of uninfected and infected badgers in the population, our SCR model provides an intuitive approach to the analysis of spatiotemporal variation in TB epidemiology in the population while accounting for uncertainty generated from the use of CR data (i.e., imperfect capture of badgers) and the limitations of diagnostic test data (i.e., imperfect knowledge of disease state). The kernel density maps generated (Figure 4) can provide a useful tool for visualizing hotspots of disease (i.e., areas with a high prevalence of infected individuals) or guiding surveillance (e.g., by revealing areas with rapidly increasing or decreasing prevalence). Consequently, our study highlights the value of integrating disease status within an SCR framework for applied disease ecology more generally.

The choice of grid size is a crucial factor in this modeling framework as it can impact accuracy and computational efficiency. A smaller grid size provides finer resolution, capturing intricate details and small-scale patterns in density. However, using a smaller grid size comes at the cost of increased computational complexity and memory requirements. On the other hand, a larger grid size provides a coarser resolution that can overlook smaller-scale patterns but reduces the computational burden. Thus, it is important to strike a balance between accuracy and computational efficiency when selecting grid size. To achieve this, a sensitivity analysis can be carried out. Varying the grid size helps determine the most appropriate size and also helps ensure that the chosen grid size does not unduly influence the results. At the same time, since disease transmission is dependent on latent density, the grid size needs to be chosen such that there are adequate latent density points to serve as a covariate on disease transmission.

One caveat to our model is that we assumed individual ACs do not change over the period of study. This reflected limited badger movement as highlighted by Rogers et al. (1998) and in Figure S7. However, this assumption will be violated for species that change ACs frequently. Our modeling approach can be extended to accommodate such movement by using different state models such as the independent (Royle et al. 2014) and the Markovian random walk model (Raabe, Gardner, and Hightower 2014). We have also assumed independence between individuals in terms of the locations of their ACs, however, populations can exhibit attraction or repulsion, which means that the spatial pattern cannot be described by a homogeneous Poisson process. In these cases, our model would need to be extended using models that account for repulsion (Diana et al. 2022; Reich and Gardner 2014) and/or attraction (McLaughlin and Bar 2021).

Another avenue for future work is the modeling of disease transmission. Here we assumed that once infected an individual remained so for the rest of its life, consistent with the normal approach when modeling TB transmission in badgers. However, in other wildlife disease systems, it may be important to introduce further states to the disease model, such as a recovered state (to represent individuals in which the disease has resolved) or a vaccinated state. Such multistate disease models have been fitted to CR data (e.g., Marescot et al. 2018), and could be easily incorporated within our modeling framework.

It could also be possible to vary how disease transmission probability is associated with the spatiotemporal distribution of infected and uninfected individuals. In this paper, we used a logistic regression to investigate the effect of (latent) local density on disease transmission probability and induce heterogeneity. However, other latent variables of this type could also be considered. For example, one might consider alternative models, a model that assumes that an uninfected individual is more likely to become infected the closer it is to infected individuals, or a model that considers disease transmission probability as a function of the overlap of home range areas between an uninfected individual and surrounding infected individuals. Additionally, spatial covariates can be used to account for spatial variation in disease transmission probability as well as demographic population rates (Milleret et al. 2023). Thus, future work can be focused on developing such models and comparing model performance.

In conclusion, our SCR model provides a novel tool to investigate the relationship between population demographics, spatial behavior, and infectious disease dynamics in imperfectly sampled systems. By applying it to other host-pathogen systems, it may be possible to gain valuable insights into how spatial behavior and pathogen epidemiology are interwoven with important implications for wildlife disease ecology and management.

Data Availability Statement

The data that support the findings of this study are available on request from the corresponding author. The data are not publicly available due to privacy or ethical restrictions.

References

Albery, G. F., L. Kirkpatrick, J. A. Firth, and S. Bansal. 2021. "Unifying Spatial and Social Network Analysis in Disease Ecology." *Journal of Animal Ecology* 90, no. 1: 45–61.

Ashford, R. T., P. Anderson, L. Waring, et al. 2020. "Evaluation of the Dual Path Platform (DPP) VetTB Assay for the Detection of *Mycobacterium bovis* Infection in Badgers." *Preventive Veterinary Medicine* 180: 105005.

Bischof, R., D. Turek, C. Milleret, T. Ergon, P. Dupont, and P. de Valpine. 2020. "nimbleSCR: Spatial Capture-Recapture (SCR) Methods Using 'Nimble'." R Package Version 0.1. 0.

Borchers, D. L., and M. G. Efford. 2008. "Spatially Explicit Maximum Likelihood Methods for Capture–Recapture Studies." *Biometrics* 64, no. 2: 377–385.

Buzdugan, S. N., T. Vergne, V. Grosbois, R. J. Delahay, and J. A. Drewe. 2017. "Inference of the Infection Status of Individuals Using Longitudinal Testing Data From Cryptic Populations: Towards a Probabilistic Approach to Diagnosis." *Scientific Reports* 7, no. 1: 1–11.

Carter, S. P., S. S. Roy, D. P. Cowan, et al. 2009. "Options for the Control of Disease 2: Targeting Hosts." In *Management of Disease in Wild Mammals*, 121–146. Tokyo, Japan: Springer Japan.

Cheeseman, C. L., and S. A. Harris. 1982. "Methods of Marking Badgers (*Meles meles*)." *Journal of Zoology* 197: 289–292.

Choquet, R., C. Carrié, T. Chambert, and T. Boulinier. 2013. "Estimating Transitions Between States Using Measurements With Imperfect Detection: Application to Serological Data." *Ecology* 94, no. 10: 2160–2165.

Dalley, D., D. Davé, S. Lesellier, et al. 2008. "Development and Evaluation of a Gamma-Interferon Assay for Tuberculosis in Badgers (*Meles meles*)." *Tuberculosis* 88, no. 3: 235–243.

de Valpine, P., D. Turek, C. J. Paciorek, C. Anderson-Bergman, D. T. Lang, and R. Bodik. 2017. "Programming With Models: Writing Statistical Algorithms for General Model Structures With NIMBLE." *Journal of Computational and Graphical Statistics* 26, no. 2: 403–413.

Delahay, R., S. Carter, G. Forrester, A. Mitchell, and C. Cheeseman. 2006. "Habitat Correlates of Group Size, Bodyweight and Reproductive Performance in a High-Density Eurasian Badger (*Meles meles*) Population." *Journal of Zoology* 270, no. 3: 437–447.

Delahay, R. J., G. C. Smith, A. I. Ward, and C. L. Cheeseman. 2005. "Options for the Management of Bovine Tuberculosis Transmission From Badgers (*Meles meles*) to Cattle: Evidence From a Long-Term Study." *Mammal Study* 30, no. Supplement: S73–S81.

Delahay, R. J., N. Walker, G. Smith, et al. 2013. "Longterm Temporal Trends and Estimated Transmission Rates for *Mycobacterium bovis* Infection in an Undisturbed High-Density Badger (*Meles meles*) Population." *Epidemiology and Infection* 141, no. 7: 1445–1456.

Diana, A., E. Matechou, J. E. Griffin, Y. Jhala, and Q. Qureshi. 2022. "A Vector of Point Processes for Modeling Interactions Between and Within Species Using Capture-Recapture Data." *Environmetrics* 33: e2781.

Drewe, J. A., A. J. Tomlinson, N. J. Walker, and R. J. Delahay. 2010. "Diagnostic Accuracy and Optimal Use of Three Tests for Tuberculosis in Live Badgers." *PLoS One* 5, no. 6: e11196.

Efford, M. 2004. "Density Estimation in Live-Trapping Studies." *Oikos* 106, no. 3: 598–610.

Efford, M. G., D. L. Borchers, and A. E. Byrom. 2009. "Density Estimation by Spatially Explicit Capture–Recapture: Likelihood-Based Methods." In *Modeling Demographic Processes in Marked Populations*, 255–269. Boston, MA: Springer.

Enøe, C., M. P. Georgiadis, and W. O. Johnson. 2000. "Estimation of Sensitivity and Specificity of Diagnostic Tests and Disease Prevalence When the True Disease State Is Unknown." *Preventive Veterinary Medicine* 45, no. 1–2: 61–81.

Ergon, T., and B. Gardner. 2014. "Separating Mortality and Emigration: Modelling Space Use, Dispersal and Survival With Robust-Design Spatial Capture–Recapture Data." *Methods in Ecology and Evolution* 5, no. 12: 1327–1336.

Fletcher, R. J., R. A. McCleery, D. U. Greene, and C. A. Tye. 2016. "Integrated Models That Unite Local and Regional Data Reveal Larger-Scale Environmental Relationships and Improve Predictions of Species Distributions." *Landscape Ecology* 31: 1369–1382.

Gallagher, J., and D. Horwill. 1977. "A Selective Oleic Acid Albumin Agar Medium for the Cultivation of *Mycobacterium bovis*." *Epidemiology and Infection* 79, no. 1: 155–160.

Gardner, B., J. Reppucci, M. Lucherini, and J. A. Royle. 2010. "Spatially Explicit Inference for Open Populations: Estimating Demographic Parameters From Camera-Trap Studies." *Ecology* 91, no. 11: 3376–3383.

Garnett, B., R. Delahay, and T. Roper. 2005. "Ranging Behaviour of European Badgers (*Meles meles*) in Relation to Bovine Tuberculosis (*Mycobacterium bovis*) Infection." *Applied Animal Behaviour Science* 94, no. 3–4: 331–340.

Gelman, A., and D. B. Rubin. 1992. "Inference From Iterative Simulation Using Multiple Sequences." *Statistical Science* 7: 457–472.

Gotway, C. A., and L. J. Young. 2002. "Combining Incompatible Spatial Data." *Journal of the American Statistical Association* 97, no. 458: 632–648.

Graham, J., G. Smith, R. Delahay, T. Bailey, R. McDonald, and D. Hodgson. 2013. "Multi-State Modelling Reveals Sex-Dependent Transmission, Progression and Severity of Tuberculosis in Wild Badgers." *Epidemiology and Infection* 141, no. 7: 1429–1436.

Hopkins, S. R., A. E. Fleming-Davies, L. K. Belden, and J. M. Wojdak. 2020. "Systematic Review of Modelling Assumptions and Empirical Evidence: Does Parasite Transmission Increase Nonlinearly With Host Density?" *Methods in Ecology and Evolution* 11, no. 4: 476–486.

Hu, H., K. Nigmatulina, and P. Eckhoff. 2013. "The Scaling of Contact Rates With Population Density for the Infectious Disease Models." *Mathematical Biosciences* 244, no. 2: 125–134.

Krkošek, M. 2010. "Host Density Thresholds and Disease Control for Fisheries and Aquaculture." *Aquaculture Environment Interactions* 1, no. 1: 21–32.

Manlove, K., E. F. Cassirer, P. C. Cross, R. K. Plowright, and P. J. Hudson. 2016. "Disease Introduction Is Associated With a Phase Transition in Bighorn Sheep Demographics." *Ecology* 97, no. 10: 2593–2602.

Marescot, L., S. Benhaiem, O. Gimenez, et al. 2018. "Social Status Mediates the Fitness Costs of Infection With Canine Distemper Virus in Serengeti Spotted Hyenas." *Functional Ecology* 32, no. 5: 1237–1250.

McCallum, H. 2016. "Models for Managing Wildlife Disease." *Parasitology* 143, no. 7: 805–820.

McCallum, H., D. M. Tompkins, M. Jones, et al. 2007. "Distribution and Impacts of Tasmanian Devil Facial Tumor Disease." *EcoHealth* 4: 318–325.

McDonald, J. L., A. Robertson, and M. J. Silk. 2018. "Wildlife Disease Ecology From the Individual to the Population: Insights From a Long-Term Study of a Naturally Infected European Badger Population." *Journal of Animal Ecology* 87, no. 1: 101–112.

McLaughlin, P., and H. Bar. 2021. "A Spatial Capture–Recapture Model With Attractions Between Individuals." *Environmetrics* 32, no. 1: e2653.

Milleret, C., S. Dey, P. Dupont, et al. 2023. "Estimating Spatially Variable and Density-Dependent Survival Using Open-Population Spatial Capture–Recapture Models." *Ecology* 104, no. 2: e3934.

O'Neill, X., A. White, C. Gortázar, and F. Ruiz-Fons. 2023. "The Impact of Host Abundance on the Epidemiology of Tick-Borne Infection." *Bulletin of Mathematical Biology* 85, no. 4: 30.

Pledger, S., K. H. Pollock, and J. L. Norris. 2010. "Open Capture–Recapture Models With Heterogeneity: II. Jolly–Seber Model." *Biometrics* 66, no. 3: 883–890.

Pollock, K. H. 1982. "A Capture-Recapture Design Robust to Unequal Probability of Capture." *Journal of Wildlife Management* 46, no. 3: 752–757.

Raabe, J. K., B. Gardner, and J. E. Hightower. 2014. "A Spatial Capture–Recapture Model to Estimate Fish Survival and Location From Linear Continuous Monitoring Arrays." *Canadian Journal of Fisheries and Aquatic Sciences* 71, no. 1: 120–130.

Reich, B. J., and B. Gardner. 2014. "A Spatial Capture-Recapture Model for Territorial Species." *Environmetrics* 25, no. 8: 630–637.

Rogers, L., C. Cheeseman, P. Mallinson, and R. Clifton-Hadley. 1997. "The Demography of a High-Density Badger (*Meles meles*) Population in the West of England." *Journal of Zoology* 242, no. 4: 705–728.

Rogers, L., R. Delahay, C. Cheeseman, S. Langton, G. Smith, and R. Clifton-Hadley. 1998. "Movement of Badgers (*Meles meles*) in a High–Density Population: Individual, Population and Disease Effects." *Proceedings of the Royal Society of London. Series B: Biological Sciences* 265, no. 1403: 1269–1276.

Royle, J., R. Chandler, R. Sollmann, and B. Gardner. 2014. *Spatial Capture-Recapture*. Waltham, Massachusetts: Elsevier, Academic Press.

Royle, J. A., R. B. Chandler, R. Sollmann, and B. Gardner. 2013. *Spatial Capture-Recapture*. Waltham, MA: Academic Press.

Royle, J. A., and R. M. Dorazio. 2012. "Parameter-Expanded Data Augmentation for Bayesian Analysis of Capture–Recapture Models." *Journal of Ornithology* 152, no. 2: 521–537.

Royle, J. A., A. K. Fuller, and C. Sutherland. 2018. "Unifying Population and Landscape Ecology With Spatial Capture–Recapture." *Ecography* 41, no. 3: 444–456.

Royle, J. A., and K. V. Young. 2008. "A hierarchical model for spatial capture–recapture data." *Ecology* 89, no. 8: 2281–2289.

Rozins, C., M. J. Silk, D. P. Croft, et al. 2018. "Social Structure Contains Epidemics and Regulates Individual Roles in Disease Transmission in a Group-Living Mammal." *Ecology and Evolution* 8, no. 23: 12044–12055.

Schaub, M., and F. Abadi. 2011. "Integrated Population Models: A Novel Analysis Framework for Deeper Insights Into Population Dynamics." *Journal of Ornithology* 152: 227–237.

Silk, M. J., D. J. Hodgson, C. Rozins, et al. 2019. "Integrating Social Behaviour, Demography and Disease Dynamics in Network Models: Applications to Disease Management in Declining Wildlife Populations." *Philosophical Transactions of the Royal Society B* 374, no. 1781: 20180211.

Silk, M. J., N. L. Weber, L. C. Steward, et al. 2018. "Contact Networks Structured by Sex Underpin Sex-Specific Epidemiology of Infection." *Ecology Letters* 21, no. 2: 309–318.

Sutherland, C., J. A. Royle, and D. W. Linden. 2019. "oSCR: A Spatial Capture-Recapture R Package for Inference About Spatial Ecological Processes." *Ecography* 42: 1459–1622.

Turek, D., C. Milleret, T. Ergon, et al. 2021. "Efficient Estimation of Large-Scale Spatial Capture–Recapture Models." *Ecosphere* 12, no. 2: e03385.

Tuyttens, F., R. Delahay, D. Macdonald, C. Cheeseman, B. Long, and C. Donnelly. 2000. "Spatial Perturbation Caused by a Badger (*Meles meles*) Culling Operation: Implications for the Function of Territoriality and the Control of Bovine Tuberculosis (*Mycobacterium bovis*)." *Journal of Animal Ecology* 69, no. 5: 815–828.

Vicente, J., R. Delahay, N. Walker, and C. Cheeseman. 2007. "Social Organization and Movement Influence the Incidence of Bovine Tuberculosis in an Undisturbed High-Density Badger *Meles meles* Population." *Journal of Animal Ecology* 76, no. 2: 348–360.

Vredenburg, V. T., R. A. Knapp, T. S. Tunstall, and C. J. Briggs. 2010. "Dynamics of an Emerging Disease Drive Large-Scale Amphibian Population Extinctions." *Proceedings of the National Academy of Sciences* 107, no. 21: 9689–9694.

Weber, N., S. Bearhop, S. R. Dall, R. J. Delahay, R. A. McDonald, and S. P. Carter. 2013. "Denning Behaviour of the European Badger (*Meles meles*) Correlates With Bovine Tuberculosis Infection Status." *Behavioral Ecology and Sociobiology* 67, no. 3: 471–479.

Weber, N., S. P. Carter, S. R. Dall, et al. 2013. "Badger Social Networks Correlate With Tuberculosis Infection." *Current Biology* 23, no. 20: R915–R916.

Woodroffe, R., C. A. Donnelly, D. Cox, et al. 2006. "Effects of Culling on Badger *Meles meles* Spatial Organization: Implications for the Control of Bovine Tuberculosis." *Journal of Applied Ecology* 43, no. 1: 1–10.

Supporting Information

Additional supporting information can be found online in the Supporting Information section.